Chemical Engineering Journal 345 (2018) 126–137

Contents lists available at ScienceDirect

Chemical Engineering Journal

journal homepage: www.elsevier.com/locate/cej

Sorption and fractionation of rare earth element ions onto nanoscale zerovalent iron particles

R.A. Crane[a,*], D.J. Sapsford[b]

[a] Camborne School of Mines, College of Engineering, Mathematics and Physical Sciences, University of Exeter, Penryn Campus, Penryn, Cornwall TR10 9FE. United Kingdom

[b] School of Engineering, Cardiff University, Queen's Building, The Parade, Cardiff CF24 3AA. United Kingdom

HIGHLIGHTS

- REE removal onto nZVI via surface mediated precipitation.
- nZVI is rapid, high capacity and able to remove REE to ultratrace concentrations.
- nZVI is selective for HREE ions in preference to LREE.
- NO_3^- can be used to control the timespan of REE retention upon nZVI.
- Spontaneous REE desorption from nZVI is a new method for REE concentration.

GRAPHICAL ABSTRACT

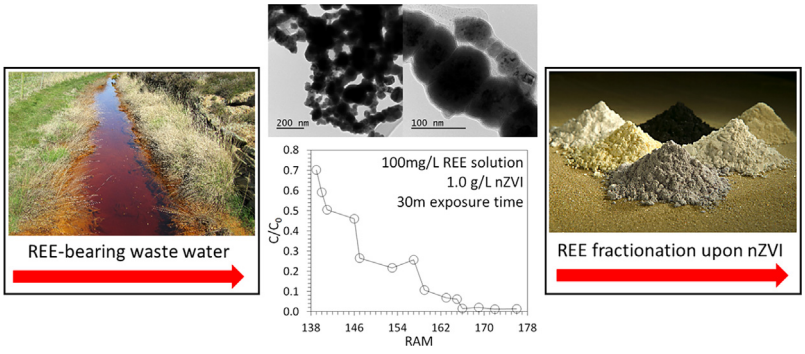

ARTICLE INFO

Keywords:
E-tech
Lanthanides
Nuclear fission waste
Water treatment
Waste valorisation
Mine waste

ABSTRACT

The removal behaviour of rare earth element (REE), (Sc, Y, La-Lu), ions onto nanoscale zerovalent iron (nZVI) particles has been investigated. Batch sorption isotherms were conducted using REE-bearing acid mine drainage (AMD) and a range of different synthetic REE solutions, which were exposed to nZVI at 0.1–4.0 g/L. Maximum adsorption capacity of Yb and La was 410 and 61 mg/g respectively (1000 mg/L $LaCl_3$ and $YbCl_3$ starting concentration, initial pH = 4.5, T = 294 K), the highest currently reported in the literature. Aqueous REE removal to ultratrace concentrations (< 1 μg/L, > 99.9% removal) was also recorded after 30 min (the first sampling interval) exposure of ≥0.5 g/L nZVI to 10 mg/L aqueous REE solutions (nitrate counterion). Similar rapidity and near-total removal ability was recorded for the exposure of nZVI to the AMD, however, a greater nZVI concentration was required, with the removal of all REEs (with the exception of La, Ce, Nd and Gd) to < 1 μg/L when exposed to nZVI at 4.0 g/L for 30 min. In all systems nZVI was selective for the removal of HREE ions in preference to LREE ions, with the mechanism determined using HRTEM-EDS and XPS analysis as *via* surface mediated precipitation. Overall the results demonstrate nZVI as exhibiting great promise as an effective and versatile agent for simultaneous REE ion recovery and fractionation.

1. Introduction

The rare earth elements (REEs), (Sc, Y, La-Lu), are a group of chemically similar elements that have gained increasing importance in recent years due to their unique functionality in many modern materials and systems, including electronics, optics, superconductors,

* Corresponding author.
E-mail address: r.crane@exeter.ac.uk (R.A. Crane).

https://doi.org/10.1016/j.cej.2018.03.148
Received 24 January 2018; Received in revised form 25 March 2018; Accepted 26 March 2018
Available online 27 March 2018

catalysts, ceramics, and agriculture. The REE global reserve is estimated to exceed 100 million tonnes [1], however, of the known 160 REE minerals, most are relatively evenly distributed in the near surface geosphere and thus unfeasible for large-scale extraction. Annual growth in the global demand for REEs is estimated to be between 8 and 11% and as such the global importance of the REEs is now becoming similar to more established commodities like oil, steel and coal [2]. Despite such demand a recent report by the Natural Environmental Research Council (NERC) has defined the REEs as the most critical chemical group in terms of global supply risk [3]. China currently produces the vast majority of all REEs from primary mining (> 85% of the global production in 2016) [4], and the worldwide recycling rate is still very low (< 1%) [3]. As global REE consumption continues to increase it is therefore inevitable that an increasing quantity of REE-bearing waste will be generated, and unless sustainable processes for their capture can be developed then this is likely to directly translate into an increase in the release of such REE into the environment from waste repositories, wastewaters and effluents. An intrinsic issue is that REEs in such emissions are often present in relatively low concentrations (e.g. < 10 mg/L) and as such conventional sorbents, such as Na-montmorillonite, activated carbon and TiO_2 are often not suitable (e.g. [5–7]). In addition the chemical similarity of the REEs dictates that even if REEs are captured their separation from each other remains a significant technical and economic challenge.

Conventional industrial-scale methodologies for REE separation from each other typically involves either liquid–liquid extraction (LLE) or supported liquid extraction (SLE) procedures, which use certain ligands (e.g. specific carboxylic acids, phosphoric acids, amines, diketones) which exhibit differences in their REE association constants (typically due to lanthanide contraction). Indeed the most common solvent currently applied in industry for REE extraction is 2-ethylhexyl phosphonic acid 2-ethyhexyl mono ester (EHEHPA, also known as PC-88A, P-507 and Ionquest 801) [8]. The main advantage of EHEHPA is the relatively large separation factors between adjacent lanthanides compared to other extractants. The intrinsic chemical similarity between the REEs, however, dictates that a large number of solvent recycling stages are still required in order to achieve high REE separation [9]. In addition the heavy REEs (HREEs) interact strongly with EHEHPA and therefore require relatively strong acid concentrations for removal [10]. For example, the separation of all 15 lanthanides typically requires both several hundred mixing and a large excess of both acid and neutralising agent (e.g. approximately 10 kg of 31 wt% HCl and 2–3 kg of NaOH is required to produce 1 kg of REE) [11,12]. An additional step to convert the extracted REEs into a solid precipitate (e.g. a sheet or ingot), such as electrowinning, is also required, which adds an extra level of financial cost and practical complexity. The EHEHPA process is therefore often regarded as not well suited for both: (i) small scale applications, such as end-of-pipe water treatment, and (ii) instances where the REEs are present at low concentrations (e.g. < 10 ppm) [10].

Instead the use of low-cost sorbents which exhibit high REE removal capacity and are also able to separate and precipitate the REEs from each other is a potentially highly useful technology. Engineered nanoparticles (ENPs) are a unique class of materials, which have received much attention in recent years for their use in a wide range of water treatment applications due to their unique properties, including extremely high surface area to volume ratio and an ability to be injected into the subsurface as a colloidal suspension. ENPs which also have magnetic properties afford the significant additional benefit of being able to be efficiently transported within the aqueous phase and then recovered (along with any sorbed metal and/or metalloid species) using a magnetic field [13–15]. Nanoscale zerovalent iron (nZVI) particles possess a core shell structure, with the core comprised of Fe^0 and a thin (often < 5 nm) oxide shell which is typically primarily comprised of magnetite [16–19]. REEs form hard Lewis acid cations and as such are known to efficiently sorb onto oxide-bearing functional groups, as such those upon the surface of nZVI. Furthermore the aqueous corrosion of nZVI results in the dynamic formation of numerous different types of (hydr)oxide corrosion products which could potentially be utilised as sorption (or desorption) and/or entrapment sites for REEs during the nZVI corrosion process. In addition the magnetic properties of nZVI are likely to enable the material to be controlled remotely using a magnetic field for the recovery of aqueous REEs from difficult to access solutions, such as nuclear fission waste. Despite such positive attributes the sorption behaviour of nZVI towards aqueous REEs remains relatively unexplored, with research on this topic currently limited, to the best of our knowledge, to one study, wherein nZVI was tested for the removal of REEs from synthetic solutions [20]. This work has been established in order to further develop a mechanistic and kinetic understanding of the sorption (and desorption) behaviour of REEs under a range of conditions including such conditions which are pertinent for the application of nZVI for the recovery of REE from wastewaters and effluents. Moreover the performance of nZVI for the recovery and retention of REEs from acid mine drainage (AMD) has also been investigated herein, which to the best of our knowledge has not yet been studied.

2. Materials and methods

2.1. Zero-valent iron nanoparticle synthesis

Pure nZVI were synthesised following the methodology first described by Glavee et al., [21] and then adapted by Wang and Zhang [22]. 7.65 g of $FeSO_4{\cdot}7H_2O$ was dissolved in 50 mL of Milli-Q water (> 18.2 MΩ cm) and then a 4 M NaOH solution was used to adjust the pH to 6.8. The salts were reduced to nZVI by the addition of 3.0 g of $NaBH_4$. The nanoparticle product was isolated from the aqueous phase *via* centrifugation (Sigma 6 K15 centrifuge, 4000 RPM for 120 s), rinsed with absolute ethanol (ratio of 50 mL/g of nZVI) and then centrifuged (Hamilton Bell v6500 Vanguard centrifuge, 6500 RPM for 120 s). This step was then repeated three times. The nanoparticles were dried in a vacuum desiccator (approx. 10^{-2} mbar) for 48 h and then stored in an argon filled (BOC, 99.998%) MBraun glovebox until required.

2.2. Experimental procedure

Four types of REE bearing solutions were used in this study: a solution containing 10 mg/L REE (Sc, Y, La-Lu) in a HNO_3 matrix with the starting pH adjusted using 0.1–4 M NaOH (hereafter termed: 10 mg/L multielement REE solution); a solution containing 100 mg/L REE (Sc, Y, La-Lu) in a HNO_3 matrix with the starting pH adjusted using 0.1–4 M NaOH (hereafter termed: 100 mg/L multielement REE solution); a mixed solution of 1000 mg/L La and Yb with chloride as the counterion and the starting pH adjusted using 0.01 M NaOH (hereafter termed: 1000 mg/L La and Yb solution); and acid mine drainage (hereafter termed AMD). The 100 mg/L multielement REE solution comprised a multi-element ICP calibration solution (QMX 700-031-015; Sc, Y, La-Lu 100 mg/L; matrix: 5% HNO_3), with the 10 mg/L multielement REE solution synthesised *via* dilution using Milli-Q water (> 18.2 MΩ cm). 0.1 M $NaClO_4$ (Sigma Aldrich, 410241) was also added as a background electrolyte. The mixed 1000 mg/L La and Yb solution was synthesised *via* the dissolution of $LaCl_3$ ($LaCl_3{\cdot}xH2O$, Fisher Scientific: 10005690) and $YbCl_3$ ($YbCl_3{\cdot}6H_2O$, Sigma Aldrich: 337927) salts into Milli-Q water. 0.1 M $NaClO_4$ (Sigma Aldrich, 410241) was also added as a background electrolyte and the pH was adjusted using 0.01 M NaOH. The AMD was collected from Parys Mountain which is a disused open cast Cu-Pb-Zn mine on Anglesey (Wales, UK). The sampling location was the Duffryn Adda adit at GPS location: 53°23′40.96 N, 4°21′01.80 W. Samples were sealed in high-density polyethylene bottles (without headspace) and stored at 4 °C until required. Prior to its use the AMD was allowed to equilibrate in the ambient laboratory (temperature = 20 ± 0.5 °C) for 24 h.

Unless specified differently all solutions were 200 mL in volume and housed in 250 mL clear soda lime glass screw capped jars (Fisher

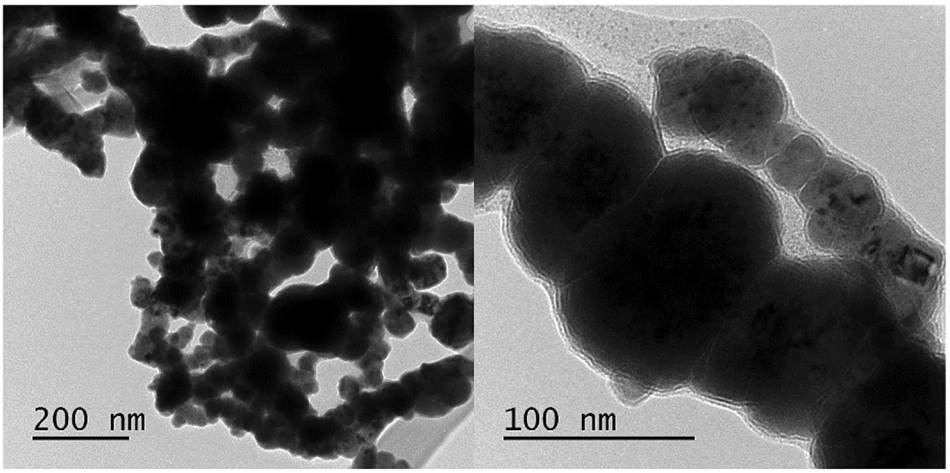

Fig. 1. HRTEM images of the as-formed nZVI.

Scientific, 11704329). Following nZVI addition the batch systems were immediately sonicated for 120 s using an ultrasonic bath (Grant, XB3). Each system was then sealed (using the screw cap of the jar) and placed on the benchtop in the open laboratory. Periodic sampling of dissolved oxygen (DO), oxygen reduction potential (ORP) and pH was conducted by gently agitating each batch system in order to ensure homogeneity. The pH, Eh and DO probes were calibrated prior to each measurement. The measured ORP values were converted to Eh by subtracting the difference between the measured ORP of the reference solution and the theoretical ORP of the reference solution (220 mV). 5 mL aqueous-nZVI suspensions were periodically taken using an auto-pipette. The extracted suspensions were centrifuged at 4000 RPM (3077*g*) for 240 s after which the supernatant became clear (i.e. all of the nZVI was centrifuged to the bottom of the vial). The supernatant was then extracted using a 10 mL syringe and filtered through a cellulose acetate filter 0.2 μm filter. The filtrate was prepared for inductively coupled plasma mass spectroscopy (ICP-MS) by the additional of HNO_3 at a concentration of 2% by volume. The solid was prepared for X-ray diffraction (XRD) or high-resolution transmission electron microscopy (HRTEM) analysis by rinsing with 40 mL of absolute ethanol and then centrifuging at 4000 RPM (3077*g*) for 240 s. The supernatant was then decanted. This step was then repeated twice more. The resultant solid material was then pipetted onto a glass optical microscope slide (Agar Scientific, G251P) and a copper coated holey carbon film (TAAB, C062/C) for XRD and HRTEM respectively. Samples were then dried in a vacuum chamber at $< 1 \times 10^{-2}$ mbar for a minimum of 2 h prior to analysis. All sorption–desorption experiments were conducted at room temperature (measured to be 20 °C ± 1 °C) and ran as duplicates, with the average data used to create the figures/tables displayed herein. A control (solution not exposed to the nZVI) was also included for each type of solution and was both monitored for pH, Eh and DO and aliquots were taken for inductively coupled plasma mass spectrometry (ICP-MS) analysis at the same time intervals as specified above.

2.3. Analysis techniques

A Phillips Xpert Pro diffractometer with a CoKa radiation source was used for XRD analysis (generator voltage of 40 keV; tube current of 30 mA). XRD spectra were acquired between 2 h angles of 10–90, with a step size of 0.02 and a 2 s dwell time. BET surface area analysis was performed using a Quantachrome NOVA 1200 surface area analyser, with N_2 as the adsorbent and following a 7 point BET method. Prior to analysis the samples were degassed under vacuum (~10 − 2 mbar) for a 24 h period at a temperature of 75 °C. Samples were run as triplicates with the average recorded. ICP-MS analysis was performed using a Thermo X Series 2 Inductively-Coupled Plasma Mass Spectrometer. The limit of detection (LOD) and limit of quantification (LOQ) for all elements analysed was ≤0.012 and ≤0.041 ppb respectively. HRTEM analysis was performed in a JEOL JEM-2100 microscope at 200 kV. Energy dispersive spectroscopy (EDS) analysis and mapping was performed using Oxford Instruments X-MaxN analyzer and Aztec software. X-ray photoelectron spectroscopy (XPS) spectra were collected using a Thermo K-Alpha+ spectrometer. Spectra were collected at a pass energy of 40 eV for narrow scans and 150 eV for survey scans with a 0.1 and 1 eV step respectively. Charge neutralisation was achieved using a combination of low energy electrons and argon ions. Spectra were quantified by first performing a scan from binding energy of 0–1350 eV. The regions with significant signal to noise ratio (corresponding to elements: B, C, O, Na and Fe) were then selected for quantification in CasaXPS using Scofield sensitivity factors and an energy dependence of −0.6. All binding energy values were referenced to the adventitious hydrocarbon C1s peak at 284.8 eV.

3. Results and discussion

3.1. Characterisation of the as-formed nZVI

Characterisation of the unreacted nZVI was performed using BET surface area analysis, HRTEM, XRD and XPS. BET surface area analysis determined the surface area of nZVI as 48.7 m^2/g. HRTEM analysis determined that the nanoparticles were spherical and typically within a size range of 10–150 nm and with a mean diameter of 67.9 nm for nZVI (Fig. 1). Each individual nZVI particle is recorded to contain a discrete 3–5 nm thick outermost layer (density contrast), which is attributed to be the presence of an oxide shell surrounding the Fe^0 core. In addition dark mottles were recorded within the metallic cores which indicates that individual particles are either polycrystalline or comprised isolated metal crystals in an otherwise amorphous matrix. The nZVI were also recorded as aggregated into chains and rings due to their high surface energy and magnetic properties [23]. XRD analysis confirmed the major crystalline component to be α-Fe^0, although only a single broad diffraction peak at 52.381° 2θ was recorded for the nZVI (the 110 lattice reflection) which indicates that the nZVI are relatively amorphous (Fig. 2). XPS analysis recorded the outer surface as comprised of a mixed valent (Fe^{2+}/Fe^{3+}) oxide (Fig. 2) overlaying a Fe^0 core. Given the mean free path of Fe is equivalent to approximately 6 atomic layers, this detection of Fe^0 in the XPS analysis volume therefore indicates that the oxide thickness of the nZVI is less than approximately 5 nm, which corroborates the aforementioned nZVI oxide thickness measurement using HRTEM. The results are summarised in Table 1 and concur with previous characterisation studies of nZVI (e.g. [24–28]).

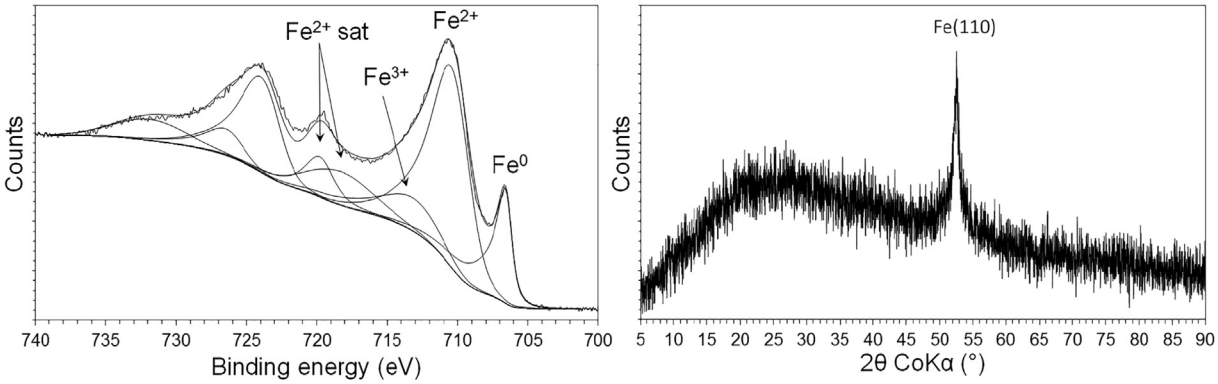

Fig. 2. Curve fitted XPS (LHS) and XRD (RHS) spectra for the as-formed nZVI.

Table 1
Bulk and surface properties of the nZVI. *A significant proportion of the carbon detected is likely to be adventitious carbon. The particle size distribution was calculated using measurements taken from the HRTEM images.

Parameter	Analysis technique	nZVI
Particle size distribution (%)	HRTEM	0–50: 26.4 50–100: 63.1 > 100: 10.5
Average particle size (nm)	HRTEM	67.9
Bulk composition	XRD	α-Fe^0
Oxide thickness (nm)	HRTEM, XPS	3–5
Surface composition	XPS	B: 14.3 C: 7.1 O: 49.3 Na: 7.3 Fe: 22.0
Fe stoichiometry ($Fe^0/Fe^{2+}+Fe^{3+}$)	XPS	0.27
Fe stoichiometry (Fe^{2+}/Fe^{3+})	XPS	3.87
Specific surface area (m^2/g)	BET	48.7

3.2. Characterisation of the AMD

Prior to nZVI addition the pH, Eh and DO of the AMD was measured along with the concentrations of dissolved metals and metalloids using ICP-OES. The water was acidic (pH = 2.52) and oxygen-rich (DO and Eh of 565 mV and 8.98 mg/L respectively). Aqueous REE concentrations in the AMD are displayed in Table 2, with all other notable metals and metalloids determined using ICP-OES is displayed in Table S1.

Table 2
Concentrations of REEs in the AMD as determined using ICP-MS.

Element	Concentration (μg/L)
Sc	156.4
Y	220.4
La	80.0
Ce	220.8
Pr	35.8
Nd	152.6
Sm	56.4
Eu	11.2
Gd	60.2
Tb	12.4
Dy	53.2
Ho	12.2
Er	27.4
Tm	6.2
Yb	20.4
Lu	18.4

3.3. Eh, pH and DO

For all experimental systems, the addition of nZVI to the water samples resulted in a rapid decrease in Eh and DO and an increase in pH (Figs. S1 and S2). Eh minima was recorded within the first 2 h of reaction in all systems studied, with 74, 37, -302 and −456 mV recorded for the 10 mg/L REE multielement solution (HNO_3 matrix, starting pH adjusted using NaOH) when exposed to nZVI at 0.1, 0.2, 0.5 and 1.0 g/L respectively after 1 h reaction, compared to −112 mV recorded for the 100 mg/L REE multielement solution (HNO_3 matrix, starting pH adjusted using NaOH) when exposed to nZVI at 1.0 g/L, −121 mV recorded for the 1000 mg/L La and Yb solution (chloride counterion, starting pH adjusted using NaOH) when exposed to nZVI at 1.0 g/L, and 148, −212, −284 and −493 mV recorded for the AMD when exposed to nZVI at 0.1, 0.2, 0.5 and 1.0 g/L respectively. Similarly in all systems a transition to near-zero DO (< 0.01 mg/L) was observed, with the exception of 10 mg/L REE solutions which were exposed to 0.1 and 0.2 g/L nZVI and AMD exposed to 0.5 g/L nZVI (which is attributed to the insufficient nZVI mass not being able to sufficiently scavenge all of the DO present).

Maximum pH was also recorded within the first 4 h of reaction in all systems studied (Figs. S1 and S2) with 7.13 and 7.54 recorded after 1 h of exposure of 0.1 and 0.2 g/L nZVI respectively to the 10 mg/L REE multielement solution, compared to 8.49 and 9.59 recorded after 2 h of exposure of 0.5 and 1.0 g/L nZVI respectively. A pH of 7.35 was recorded after 30 min exposure of 1.0 g/L nZVI to the 100 mg/L REE multielement solution compared to 6.89 recorded after 2 h exposure for the 1000 mg/L La and Yb chloride solution. Moreover a pH of 4.28 was recorded after 1 h exposure of 0.5 g/L nZVI to the AMD, compared to 5.85 recorded after 4 h exposure of 1.0 g/L nZVI, and 6.30 and 6.56 recorded after 2 h exposure of 2.0 and 4.0 g/L nZVI respectively.

This behaviour is attributed to the rapid oxidation of nanoparticulate surfaces during their initial exposure to the REE-bearing solutions, consuming DO and H^+ and decreasing the system Eh of the system. Following this a gradual reversal to pH, Eh and DO conditions similar to pre-nZVI exposure was observed in all systems, which is attributed to the reactive exhaustion of the nZVI (i.e. total transformation of Fe^0 to Fe^{2+} and/or Fe^{3+} (hydr)oxide products) and ingress of atmospheric oxygen.

3.4. ICP-MS/OES

Addition of the nZVI to the REE bearing solutions resulted in a decrease in aqueous REE concentrations in all systems studied (Figs. 3–6 and Fig. S3-6). A similar decrease was also recorded for Al, Cd and Cu within the AMD (Tables S2–5), which agrees with previous work [29]. Most significant REE removal (and simultaneous Fe dissolution) was recorded for systems exposed to the highest mass of nZVI, with removal to trace concentrations (i.e. < 1 μg/L) of all REEs

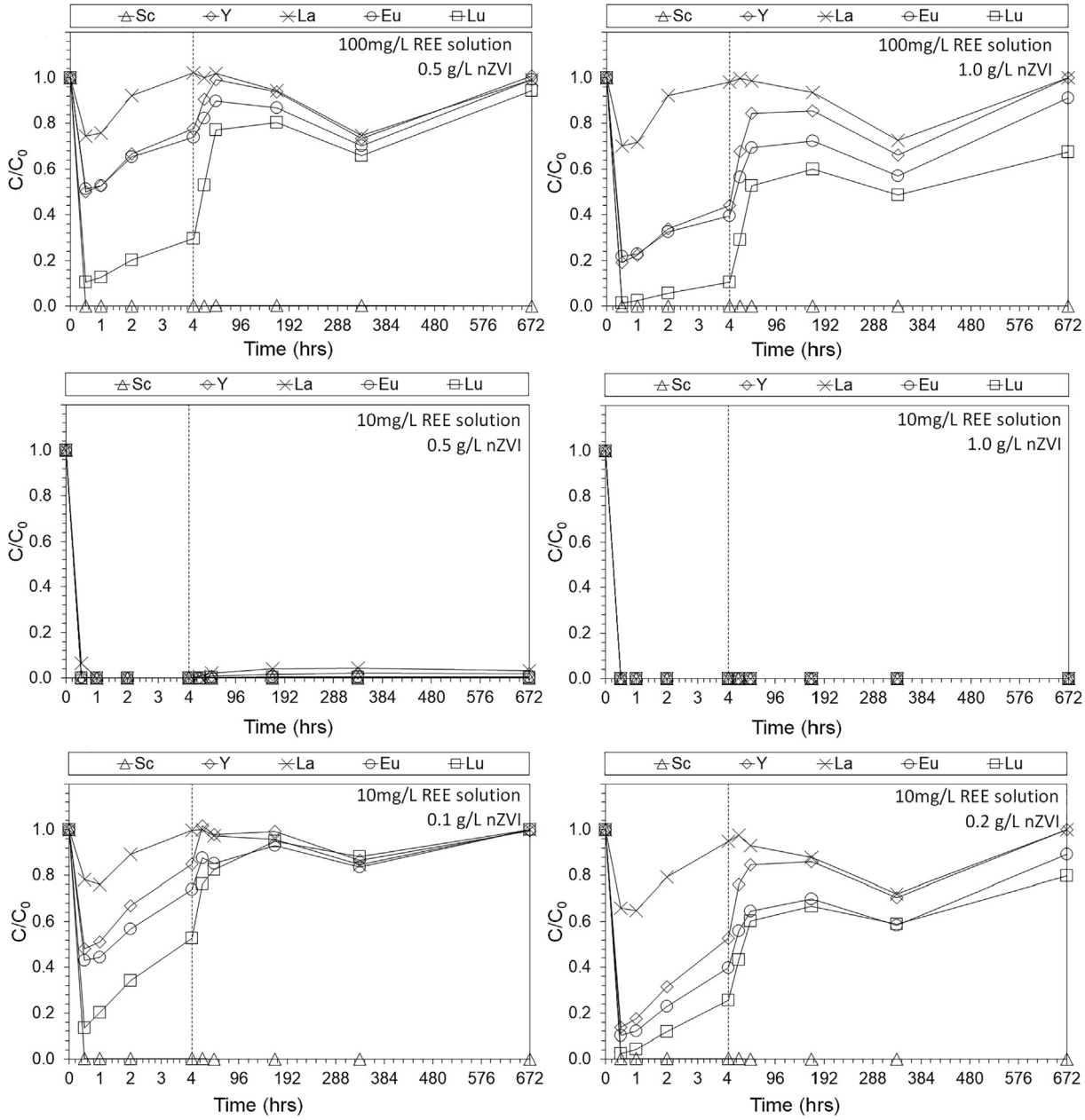

Fig. 3. Normalised Sc, Y, La, Eu and Lu concentrations (C/C_0) as a function of time for the synthetic REE solutions (HNO_3 matrix, starting pH adjusted using NaOH). Starting pH, Eh and DO was 4.7, 415 mV and 10.3 mg/L, and 4.9, 420 mV and 9.2 mg/L respectively for the 100 mg/L REE solution and 10 mg/L REE solution respectively (see Fig. S1).

recorded following exposure of the 10 mg/L multielement REE solution (HNO_3 matrix) to nZVI at a concentration of 1.0 g/L for 30 min (Fig. 3). Similarly, removal of all REEs to < 1 µg/L, with the exception of La, Ce, Nd and Gd, were recorded when the AMD was exposed to 4.0 g/L nZVI for 30 min (Fig. S3).

Figs. 4 and 5 display normalised aqueous REE concentrations (C/C_0) determined for the 10 and 100 mg/L multielement REE solutions and the AMD respectively following exposure to the nZVI for between 0.5 and 24 h. It can be observed that nZVI consistently fractionates the REEs by preferentially removing lower ionic radius REEs (i.e. the HREEs) from the aqueous phase in preference to higher ionic radius REE (i.e. the LREEs). Moreover Fig. 6 displays normalised aqueous La and Yb concentrations following exposure of nZVI (at 1.0 g/L) to a 1000 mg/L La and Yb chloride solution, with nZVI recorded as selective for the removal of Yb in preference to La, with maximum uptake of 410 and 61 mg/g recorded for each lanthanide respectively. To the best of our knowledge this is the highest Yb removal capacity currently reported for any material. Examples of Yb removal capacities in the literature include: 121.2 mg/g for removal onto brown marine alga, *Turbinaria conoides* [30]; 33.9 mg/g for removal onto nanoscale silica [31]; and 322.7 mg/g for removal onto SQD-85 resin [32]. In addition, kinetic sorption data (t/q vs t) indicates that the Yb uptake rate is psuedo-second order with respect to the available surface sites Fig. S4) in a linear relationship ($R^2 = 0.993$). It has been reported that when the REEs are in the presence of anions such as those investigated herein (i.e. chloride, nitrate, hydroxide) a wide variety of chemical species can form, such as $Ln(OH)_2^+$, $Ln(OH)_4^-$, $LnCl_3{\cdot}xH_2O$, $Ln(NO_3)_3{\cdot}H_2O$, in addition to polymeric species. It has been documented that the REEs form relatively weak outer-sphere complexes with chloride and as such the speciation for chloride containing systems investigated here (Fig. 6) is likely to be dominated by hydroxyl species [20]. The dominant oxidation state of aqueous REE in such systems is likely to have been

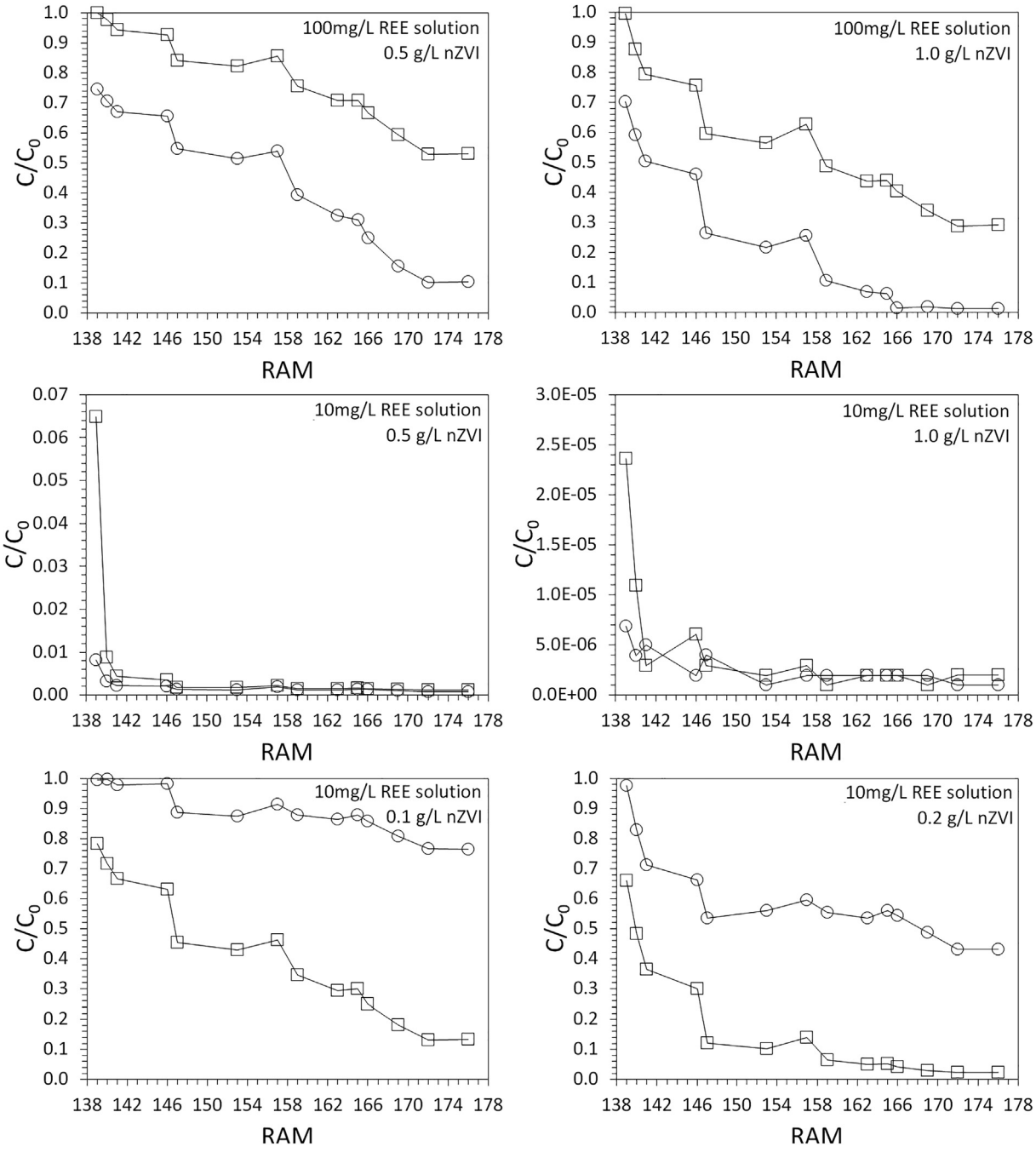

Fig. 4. Normalised aqueous lanthanide concentrations (C/C_0) in the synthetic REE solutions (HNO_3 matrix, starting pH adjusted using NaOH) following exposure to nZVI after 0.5 h (square markers) and 24 h (circle markers). Starting pH, Eh and DO was 4.7, 415 mV and 10.3 mg/L, and 4.9, 420 mV and 9.2 mg/L respectively for the 100 mg/L REE solution and 10 mg/L REE solution respectively (see Fig. S1).

trivalent and such REE ions are therefore likely to have behaved as hard acids that can bind strongly to oxides and hydroxides. The zerovalent iron core within nZVI comprises an electron source that can reduce ions possessing higher standard reduction potentials than Fe^0 (−0.41 V). REEs exhibit standard electrode potentials lower than −0.41 V and as such are not thermodynamically favourable to undergo chemical reduction when exposed to Fe^0. Instead REE uptake onto nZVI is anticipated to occur predominantly *via* sorption onto the (hydr)oxide shell which surrounds each nZVI particle (*via* the aforementioned hard acid-hard base interaction). In addition at a pH greater than approximately 7.5 the diminishing solubility of REE dictates that precipitation could also have spontaneously occurred [33]. These mechanisms, however, do not to take into consideration the preferential uptake of HREE in preference to LREE recorded herein. It is well documented that the speciation and associated aqueous stability of REEs is heavily dependent upon REE relative atomic mass (RAM) with the HREEs favouring the formation of less sterically crowded complexes (e.g. $REECl_4^-$) compared to larger complexes which predominate for the LREEs. Moreover it is well known that the differences in coordination numbers between the LREEs and the HREEs impacts their hydration number, with the number of REE aquo-ions decreasing from typically 9 for LREEs to typically 8 for HREEs (with a transition region from Sm to Gd) [34]. This higher coordination number could therefore potentially preferentially restrict the bulk diffusion of LREE compared to HREE onto nZVI sorption sites. In addition the formation constants of REE complexes are known to be effected by REE ionic radius contraction,

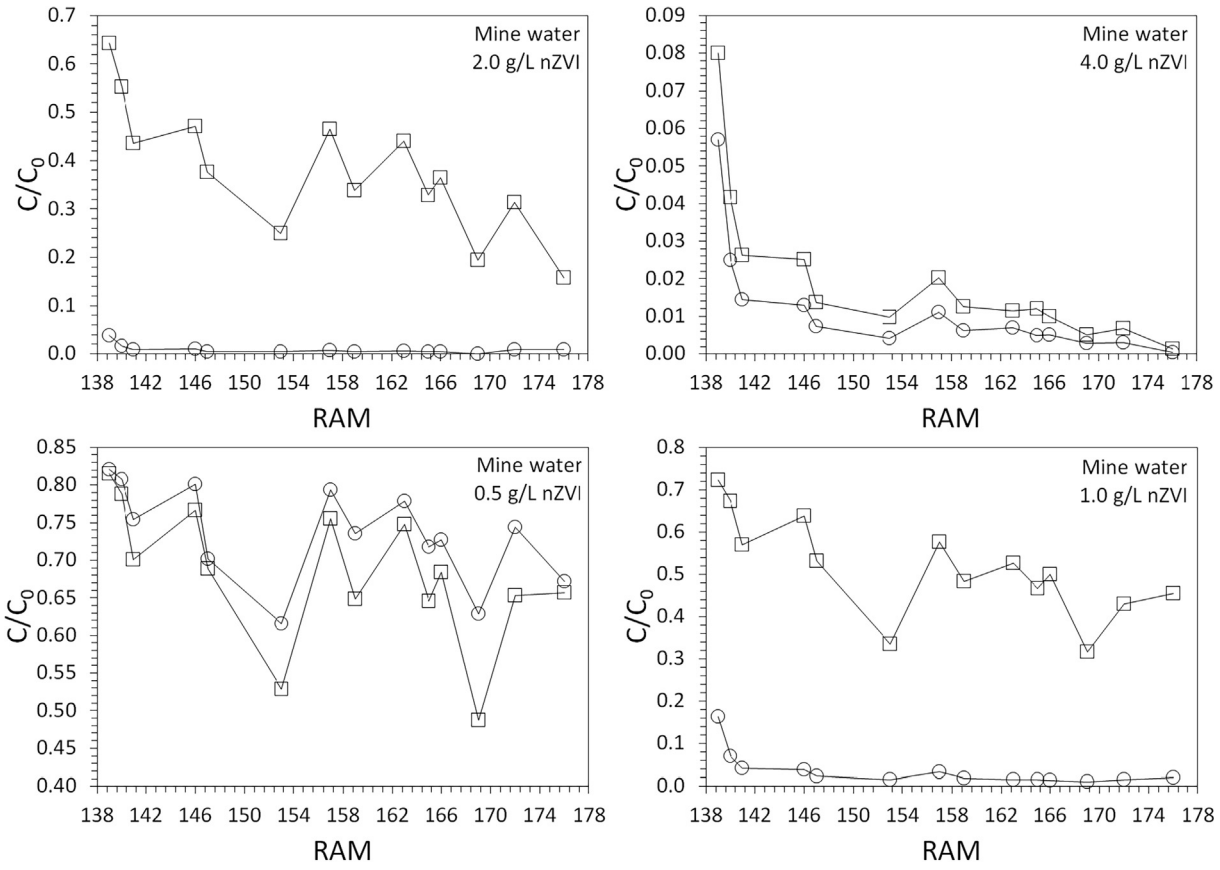

Fig. 5. Normalised aqueous lanthanide concentrations (C/C_0) in the AMD following exposure to nZVI after 0.5 h (square markers) and 24 h (circle markers). Starting pH, Eh and DO was 2.5, 565 mV and 9.0 mg/L respectively (see Fig. S1).

with an increase in such formation constants typically noted from La-Lu and thereby likely increasing the electrostatic attraction of HREE to nZVI surfaces [34]. Moreover it is also clear from the results presented herein that charge density played a key role in the uptake of HREE in preference to LREE onto nZVI because such fractionation was more evident for the batch systems containing greater starting concentrations of REE (Figs. 3, 4 and 6), which has also been noted elsewhere [20].

We therefore hypothesise that the preferential removal of HREEs onto nZVI recorded herein at pH < 8 is likely to be due to their preferential diffusion from outer-sphere coordination into inner-sphere coordination at the oxyhydroxyl/oxide interface (upon the nZVI surface) due to their higher lanthanide cation charge density and associated ability to form less sterically crowded complexes than the LREEs. However, at pH greater than approximately 7 it is likely that the precipitation of insoluble REE hydroxides is likely to have also played a key role, i.e. as $REE(OH)_{3(s)}$. At acidic pH and when SO_4^{2-} is present in appreciable concentrations (e.g. > 1 mM) $REESO_4^+$ complexes typically dominate over other common REE complexes (e.g. REE^{3+}, $REECO_3^+$, $REE(CO_3)_2$, $REE(OH)_3$) [35]. As such the REEs present in the AMD herein is likely to also have been positively charged with the selective removal of the HREEs likely to have been *via* a similar mechanism.

Near total REE removal (> 99.9%) was maintained until the end of the 672 h reaction period for the 10 mg/L multielement REE solutions that were exposed to nZVI at concentrations of 0.5 and 1.0 g/L. In contrast significant REE re-release (i.e. re-dissolution) was recorded for all other batch systems. It can be observed in Figs. 4, 5 and S3-5 that no clear trend in the selectivity of this desorption process (i.e. LREEs vs HREEs) can be confirmed.

Metal and metalloid desorption from nZVI is a phenomenon and has been previously observed for a number of different metals, including Cu and U, and in all instances (including herein), is attributed to the reactive exhaustion of the nZVI and consequent reversal of the solution chemistry to pre-nZVI-DE addition conditions. This results in the oxidative dissolution and/or desorption of metals as pH reverted to lower values and Eh increased in response to atmospheric oxygen ingress [17,29]. This interesting phenomenon could represent a new mechanism to concentrate and/or fractionate REEs as a function of ionic radius (see Section 4 for further discussion). In contrast the retention of REEs throughout the entire 672 h reaction period recorded for the 10 mg/L multielement REE solutions (HNO_3 matrix) that were exposed to nZVI at concentrations of 0.5 and 1.0 g/L provides evidence that the presence of a NO_3^- counterion could inhibit REE desorption from nZVI. This has been noted elsewhere for the removal of Cu and Zn, where it was determined that NO_3^- acted to passivate nZVI (following Cu and Zn removal) and thereby increase the corrosion lifespan of Fe^0 compared to other common groundwater anions (such as chloride) [26]. The results presented herein provide additional validation of this finding and demonstrate that it is also applicable for the REEs.

3.5. XRD

Fig. S7-9 display XRD data for the nZVI extracted at periodic intervals during its exposure to 10 mg/L multielement REE solutions (HNO_3 matrix), 100 mg/L multielement REE bearing solutions (HNO_3 matrix) AMD and the mixed solution of 1000 mg/L La and Yb chloride respectively. Exposure of the nZVI to the different solutions resulted in distinctly different corrosion pathways for the nanomaterial. The most rapid nZVI aqueous corrosion (i.e. exhaustion of the Fe^0 core) was recorded for the nZVI when exposed to the AMD and also when exposed to the mixed solution of 1000 mg/L $LaCl_3$ and $YbCl_3$, with no clear evidence of crystalline Fe^0 (i.e. a $Fe^0(110)$ lattice reflection) remaining

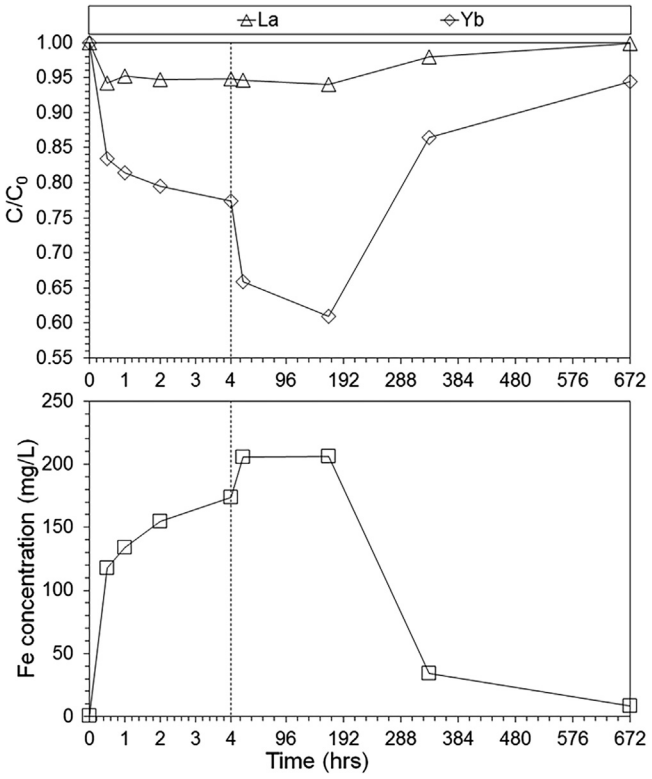

Fig. 6. Normalised aqueous La and Yb concentrations following exposure to nZVI at 1.0 g/L. Starting La and Yb concentrations were 1012.0 and 1049.4 mg/L respectively (chloride counterion, starting pH adjusted using NaOH). Starting pH, Eh and DO was 4.5, 340 mV and 10.0 mg/L respectively (see Fig. S2).

after 168 h in all systems. Instead a transition to lepidocrocite (γ-FeOOH) and goethite (α-FeOOH) was recorded for nZVI exposed to the 1000 mg/L $LaCl_3$ and $YbCl_3$ and AMD respectively. In contrast crystalline Fe^0 was recorded as present throughout the entire 672 h reaction period for the nZVI that were exposed to both 10 mg/L and 100 mg/L REE solutions (HNO_3 matrix) which is attributed to the passivation of the nZVI surface by NO_3^-. This result is in agreement with aforementioned enhanced retention of REEs upon the nZVI (as a solid precipitate) when NO_3^- is also present as a counterion (as recorded in Section 3.4.). In particular it has been suggested that NO_3^- acts to passivate nZVI *via* fostering the formation of surface oxides (namely: Fe_3O_4/γ-Fe_2O_3) in preference to hydroxides (e.g. γ-FeOOH/α-FeOOH) [26]. The detection of crystalline Fe_3O_4 in Fig. S7 supports this hypothesis.

3.6. HRTEM

Fig. 7 compares HRTEM images of the nZVI after exposure for 4, 24 and 168 h to the mixed 1000 mg/L La and Yb chloride solutions and to the AMD. HRTEM images of nZVI extracted after 4, 24, 168 and 672 h from the mixed 1000 mg/L La and Yb solution along with corresponding EDS maps are displayed in Fig. 8. Additional HRTEM-EDS data are displayed in Figs. S10-21. It can be observed that following exposure to the mixed 1000 mg/L La and Yb solution a proportion of the nZVI transformed into hollow spheres, which has been noted elsewhere and likely to have occurred *via* the outward transport of Fe ions through the (hydr)oxide layer [36]. The cavity sizes are approximately 20–60% of the size of the initial nZVI particle. The nZVI were also found to occur fused together into rings with the joining boundary between each nanoparticle subsequently collapsing allowing the formation of hollow nZVI tubes. The tubes and hollow spheres were then also observed to collapse with the subsequent emergence of iron (hydr) oxide "needles." The needles are observed to propagate radially from the nZVI and grow to lengths substantially longer then the diameter of the as-formed nZVI. ICP-MS data displayed in Section 3.4. shows that after prolonged periods of exposure time (> 168 h) of nZVI to REE solutions significant desorption of both La and Yb occurs. This correlates well with the EDS data (Table 3) and suggests that their desorption might have been caused by this (hydr)oxide needle crystallization (for example by a change in charge density). During the latter stages of the reaction the needles are recorded to develop evenly spaced laminations (along the long edge of each needle), with a morphology that is typical of lepidocrocite (γ-FeOOH), which is a common corrosion product of Fe^0 in Cl^- bearing solutions and in agreement with the XRD data (Section 3.5.) [18].

In contrast no hollow spheres were observed for the nZVI when exposed to the AMD (Fig. 7), with the nZVI instead recorded to directly form amorphous "needles." This is likely due to impurities in the AMD preventing the crystallization of a single iron-bearing corrosion product phase. The EDS maps of the nZVI extracted from the mixed 1000 mg/L $LaCl_3$ and $YbCl_3$ solution provide clear evidence that the uptake of La and Yb onto nZVI is a surface mediated process, with such sorption occurring concurrent with the aqueous corrosion of the nZVI.

3.7. XPS

Fig. 9 displays XPS La $3d_{5/2}$, Yb $4p_{3/2}$, Cl 2p and O1s photoelectron spectra recorded for nZVI which were extracted from the mixed 1000 mg/L La and Yb chloride solutions for 4, 24, 168, 336 and 672 h, with quantification data listed in Table S6. The La 3d spectra were asymmetric, with curve fitting yielding two photoelectron peaks centred at binding energies of 835.2 ± 0.05 eV and 839.0 ± 0.05 eV, which is attributed to trivalent La. The magnitude of the multiplet splitting was 3.8 ± 0.05 eV which indicates that the La was not likely present as an oxide (i.e. La_2O_3), which is known to typically exhibit La $3d_{5/2}$ multiplet splitting of ~4.6 eV [37]. Instead it is likely that it was present as either a hydroxide (i.e. $La(OH)_3$) or a chloride (e.g. $LaCl_3$), which are known to exhibit multiplet splitting of ~3.9 eV [37]. In addition, La_2O_3 and Yb_2O_3 are known to exhibit an O1s photoelectron peak within the binding energy range of ~528.5–529.2 eV [37], which was not detected. Instead two photoelectron peaks were recorded as centred at 529.8 ± 0.05 eV and 531.3 ± 0.05 eV which is attributed to O^{2-} (most likely derived from an Fe oxide) and OH^- respectively (e.g. La, Yb and/or Fe hydroxides). When comparing the La $3d_{5/2}$ data to spectra obtained for $LaCl_3{\cdot}xH_2O$ salts it can be observed that photoelectron peaks were recorded as centred at relatively similar binding energies (~0.5 eV lower), which indicates that $LaCl_3$ could be present in the samples.

The Yb $4p_{3/2}$ data were recorded as relatively symmetrical with a single photoelectron peak recorded as centred at approximately 346–347 eV, which corresponds to trivalent Yb. No photoelectron peak was detected at 340 ± 0.2 eV which indicates that Yb^0 was not present. Moreover the photoelectron peak is recorded as centred ~1 eV lower than recorded for the $YbCl_3{\cdot}6H_2O$ salt, which indicates that $YbCl_3$ could be present in the samples, but likely at a relatively low concentration. The Cl 2p data indicate that a metal-chlorine bond is present although it is unclear whether this corresponds to a Fe- or a La/Yb-Cl bond. Moreover the photoelectron peaks are recorded as centred at relatively similar binding energies to those recorded for the $LaCl_3{\cdot}xH_2O$ salt, however, approximately 0.5 eV lower than the $YbCl_3{\cdot}6H_2O$ salt, which indicates that the samples could contain a greater proportion of $LaCl_3$ compared to $YbCl_3$. This corroborates with the aforementioned La $3d_{5/2}$ and Yb $4p_{3/2}$ spectra.

Overall the XPS data confirms that La and Yb are sorbed to the surface of the nZVI, and likely present as chloride and/or hydroxide surface precipitates.

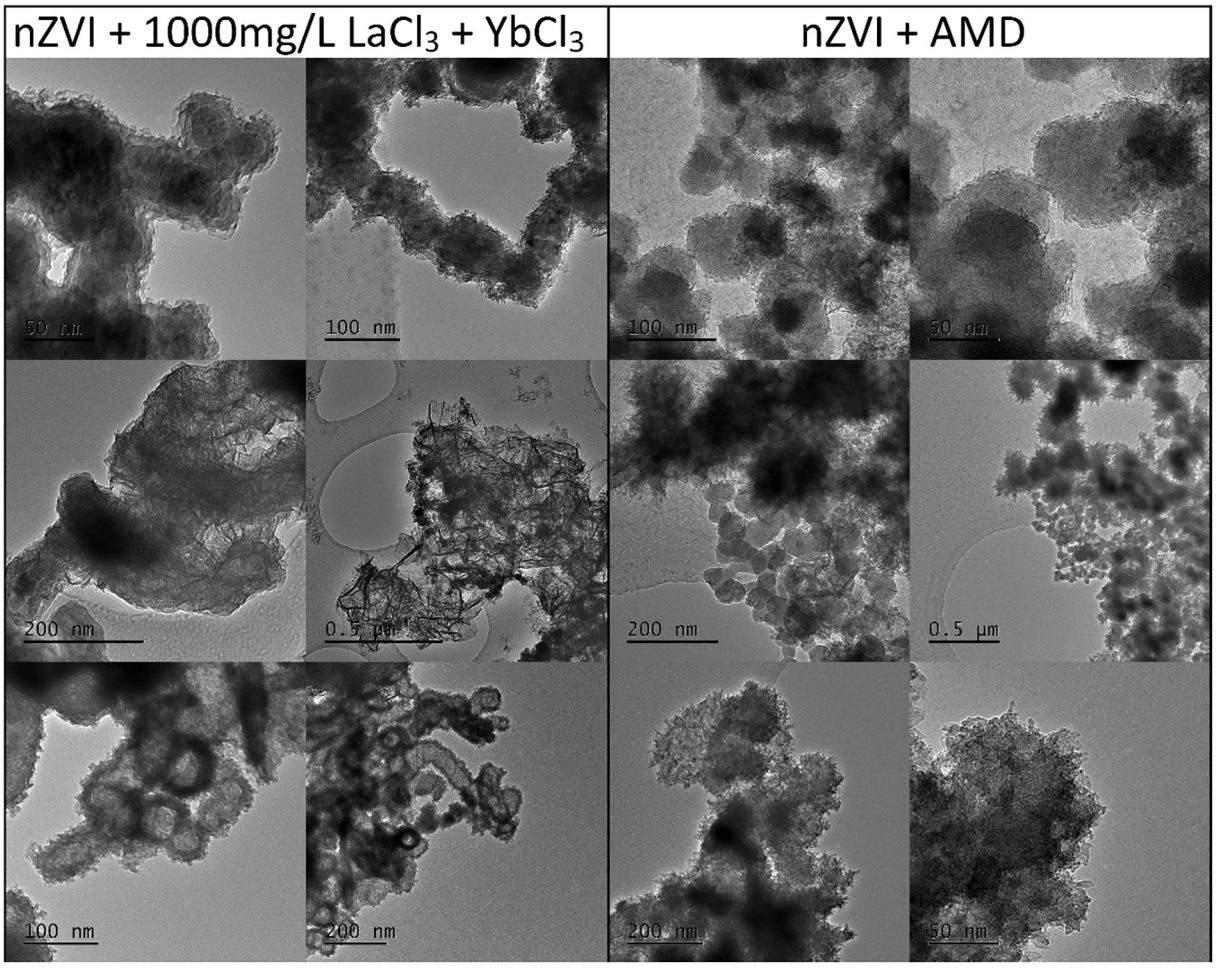

Fig. 7. HRTEM images of the nZVI following 4 (top row), 24 (middle row) and 168 h (bottom row) exposure to the 1000 mg/L $LaCl_3$ and $YbCl_3$ solution (LHS) and AMD (RHS).

4. Environmental/industrial implications

In recent years the REEs have received an increasing level of global interest due to their unique application in a wide range of modern technologies. Despite such interest NERC has recently defined the REEs as the most critical chemical group in terms of global supply risk [3]. Despite the large global cycling of REE-bearing materials and wastes an intrinsic issue associated with REE recovery from wastes (e.g. AMD) is that their concentrations are typically relatively low (e.g. < 0.1%) [38]. This is a particularly acute issue for aqueous REE bearing wastes (such as AMD) where concentrations can be as low as a few mg/L but discharge volumes can be extremely large [38]. As such there is an urgent demand for the development of low cost methodologies for the recovery of REEs from aqueous effluents. Commercially available REE recovery processes such as solvent extraction (e.g. using EHEHPA), often requiring several hundred mixing and then settling stages and also large quantities of acids and neutralising agents are not appropriate for this challenge [8]. Instead the development of low-cost and non-toxic adsorbents which have an ability to both: (i) remove REEs from relatively low concentration waste streams (e.g. < 10 mg/L); and (ii) to separate REEs from each other, would be a major technical achievement. Herein nZVI have been demonstrated as highly effective for the rapid and near-total (down to < 1 µg/L concentrations) removal of aqueous REE. The efficacy of such REE uptake has been determined to be directly dependent upon the concentration of nZVI used (Figs. 3–5). This enables greater REE removal due to the following two co-related mechanisms: (i) sorption and/or enmeshment onto and within nZVI corrosion products; and (ii) precipitation and/or coprecipitation with nZVI corrosion products due to the introduction of alkalinity into the system (due to nZVI corrosion, see Section 3.3. for details). As such it can be stated that the efficiency of nZVI for REE removal from water is likely related to the purity of the nanomaterial (i.e. the Fe^0 content) which drives both processes during nZVI aqueous corrosion.

In addition nZVI has been demonstrated to fractionate REEs, favouring the uptake of HREEs in preference to LREE and also able to desorb REEs (following near-total removal) without the input of any reagents. Moreover, it has been confirmed that the presence of NO_3^- as a REE counterion can be used to lengthen the timespan of REE retention upon nZVI (*via* passivation of nZVI aqueous corrosion), which could be utilised as a new mechanism to control this desorption process.

Due to the relatively low-cost and environmental compatibility of nZVI (it is already commercially applied in many countries for uses in *in situ* contaminated land treatment) potential applications of this new technology include the selective removal of REEs in mining (e.g. hydrometallurgical fluids, process residues, acid mine drainage), municipal (e.g. landfill leachates) and industrial wastes (e.g. nuclear fission waste). An additional highly beneficial attribute of nZVI is its (super) paramagnetic properties, which is likely to unlock a wide range of applications associated with the use of magnetic fields to control nZVI (and sorbed REEs) transport and recovery. For example, this could be of particular utility in the nuclear industry where the separation of REEs from each other (and other fission waste components) remotely would be a highly beneficial attribute in order to safeguard against harmful radiation.

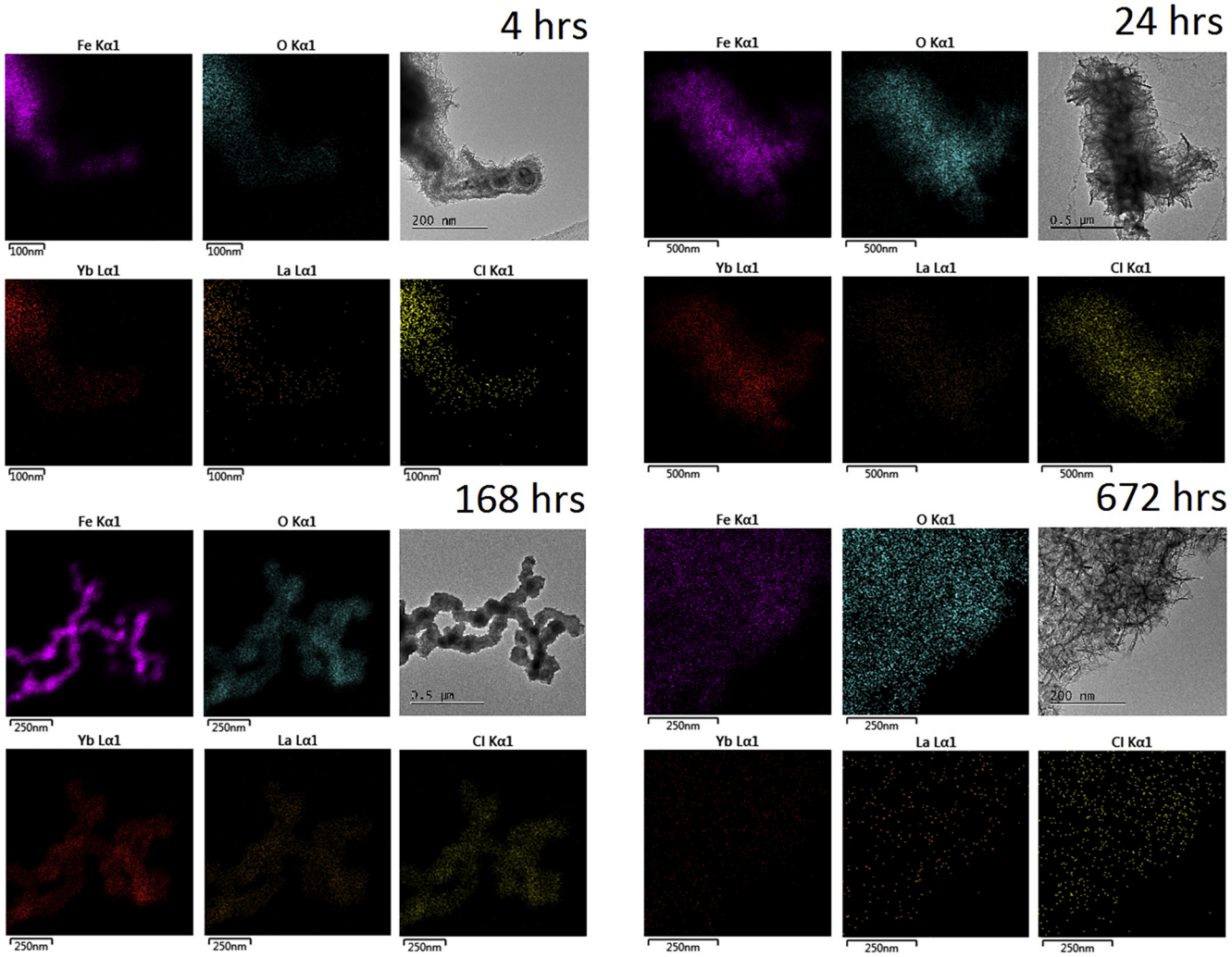

Fig. 8. HRTEM images with corresponding EDS maps of nZVI extracted from a mixed 1000 mg/L La and Yb solution (chloride counterion, starting pH adjusted using NaOH) after 4 (top left), 24 (top right), 168 (bottom left) and 672 h (bottom right). Additional HRTEM images and corresponding EDS maps are included in the supplementary data (Figs. S10–S21). EDS maps were not recorded for the nZVI extracted from the AMD and 10 mg/L REE solution because the REE concentrations were below the detection limit of the HRTEM instrument.

Table 3
Composition (by wt%) of the nZVI after exposure to a mixed 1000 mg/L La and Yb solution (chloride counterion, starting pH adjusted using NaOH) after 4, 24, 168 and 672 h as determined using HRTEM-EDS. Data corresponds to the EDS maps displayed in Fig. 8. The majority of C and Si detected is likely to have been due to sample contamination, with adventitious carbon the most likely explanation for the former.

Element	nZVI composition (wt%) after 4 h exposure to a 1000 mg/L $LaCl_3$ and $YbCl_3$ solution	nZVI composition (wt%) after 24 h exposure to a 1000 mg/L $LaCl_3$ and $YbCl_3$ solution	nZVI composition (wt%) after 168 h exposure to a 1000 mg/L $LaCl_3$ and $YbCl_3$ solution	nZVI composition (wt%) after 672 h exposure to a 1000 mg/L $LaCl_3$ and $YbCl_3$ solution
C	5.91	19.67	3.84	16.82
O	25.16	32.17	22.44	43.82
Si	0.54	0.62	0.45	1.04
S	0.31	0.43	0.49	0.22
Cl	1.49	1.90	1.87	1.07
Fe	48.90	19.94	37.39	31.78
La	1.38	0.97	3.81	0.01
Yb	16.31	24.30	29.71	1.05

5. Conclusions

Herein we have provided comprehensive evidence that nZVI is highly effective and versatile for the concurrent removal and fractionation of REE ions (favouring HREEs) from the aqueous phase. The following can be concluded:

(1) REE removal from solution can be achieved using relatively low nZVI concentrations, with removal to ultratrace levels (i.e. < 1 μg/L) at the first sampling time (30 min) recorded when nZVI were exposed to synthetic REE nitrate solutions (REE starting concentration 10 mg/L) and AMD (REE starting concentrations ranging from 36 to 200 μg/L) using nZVI concentrations of 1.0 and 4.0 g/L respectively.
(2) nZVI exhibited Ya and La removal capacities of 409.6 and 61.0 mg/g respectively when the nanomaterial was exposed to a solution of both 1000 mg/L $LaCl_3$ and $YbCl_3$ at 1.0 g/L. To the best of our knowledge this is the highest REE removal per unit surface area that currently exists in the literature.
(3) Following initial near-total removal from solution, spontaneous REE desorption was observed, with greater rapidity recorded for lower nZVI concentrations. This interesting phenomena could potentially be harnessed as a new process for the concentration of REE

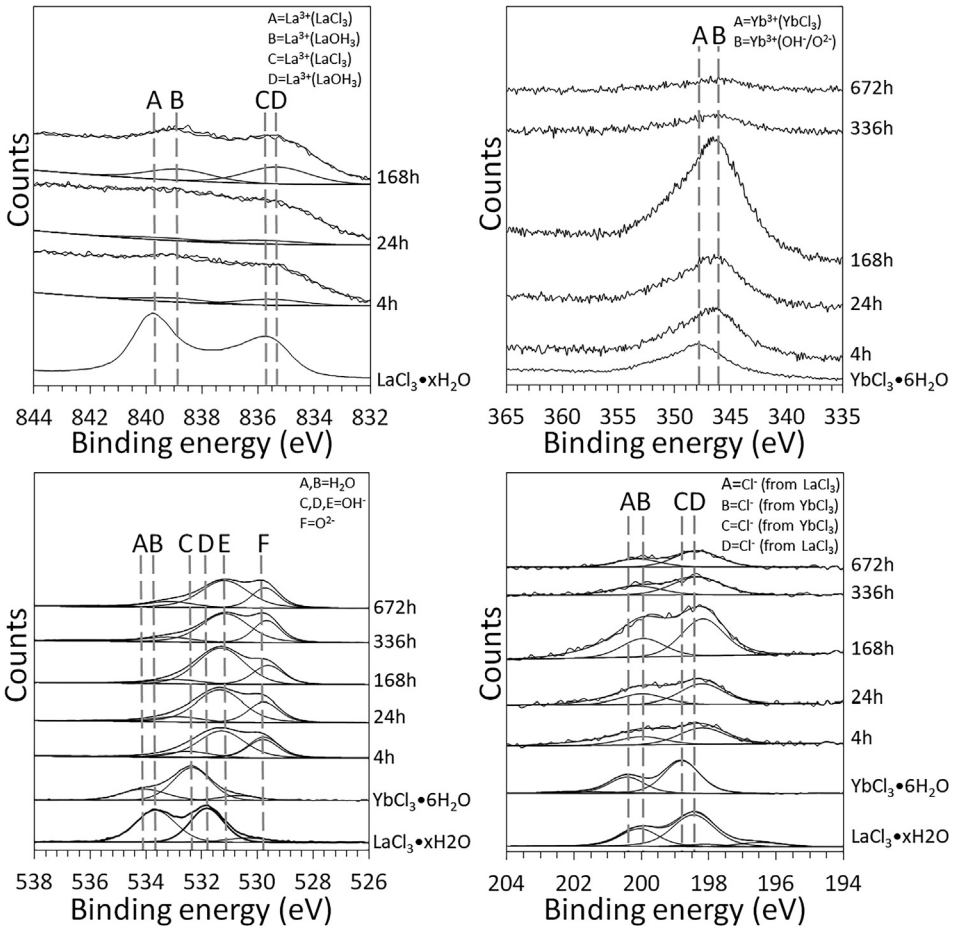

Fig. 9. Curve fitted XPS La $3d_{5/2}$, Yb $4p_{3/2}$, Cl 2p and O1s spectra recorded for nZVI following exposure to the mixed 1000 mg/L La and Yb solution (chloride counterion, starting pH adjusted using NaOH) for 4, 24, 168, 336 and 672 h. A nZVI concentration of 1.0 g/L was used. The data are stacked against spectra recorded for $LaCl_3{\cdot}xH_2O$ and $YbCl_3{\cdot}xH_2O$ salts.

ions, with the advantage being the lack of requirement for any further reagent input.

(4) nZVI results in fractionation of the REEs by favouring the uptake of HREEs in preference to the LREEs, which is attributed to a restriction of the transport (bulk diffusion) of LREEs (given their larger ionic radius than the HREEs) to nZVI sorption sites. In contrast REE desorption was not confirmed as a selective process.

(5) HRTEM-EDS and XRD analysis determined nZVI corrosion pathway as dependent on REE solution chemistry, with a transition to hollow spheres and then to lepidocrocite "needles" recorded when exposed to a mixed 1000 mg/L La and Yb solution (chloride counterion, starting pH adjusted using NaOH), compared to a transition directly to iron (hydr)oxide "needles" recorded for when exposed to AMD.

(6) HRTEM-EDS and XPS analysis determined La and Yb as sorbed to nZVI surfaces as trivalent (i.e. not chemically reduced), as hydroxides and/or chloride surface precipitate species. As such the following co-related REE removal mechanisms are likely to have occurred: (i) sorption and/or enmeshment onto and within nZVI corrosion products; and (ii) precipitation and/or coprecipitation with nZVI corrosion products due to the introduction of alkalinity into the system (due to nZVI corrosion).

Overall the results demonstrate nZVI as highly efficient (rapid, high capacity and ultratrace removal capability) for the removal of REEs from solution. Furthermore, the nanomaterial selectively removes higher value HREEs in preference to LREEs and is also able to later desorb REEs without input of any additional reagents. As such the nanomaterial holds great promise as a new technique for the selective recovery of REEs from wastewater.

Acknowledgements

We would like to thank Jeff Rowlands and Marco Santonastaso and from the School of Engineering, Cardiff University for their technical support. We would like to thank Dr Iain McDonald from the School of Earth Sciences, Cardiff University for the ICP-MS analysis. We would also like to thank Dr Thomas Davies from the Cardiff Catalysis Institute and the Cardiff Electron Microscopy Facility for the HRTEM-EDS analysis and Dr David Morgan from the School of Chemistry, Cardiff University for the XPS and BET surface area analysis. Photograph featured on the RHS of the graphical abstract is taken from the USDA [39]. This work was financially supported by the Natural Environmental Research Council (Grant number: NE/L013908/1) and the Camborne School of Mines Trust.

Appendix A. Supplementary data

Supplementary data associated with this article can be found, in the online version, at http://dx.doi.org/10.1016/j.cej.2018.03.148.

References

[1] Z.J. Chen, Global rare earth resources and scenarios of future rare earth industry, Rare Earth 29 (2011) 1–6.
[2] D. Kifle, H. Sverdrup, D. Koca, G. Wibetoel, A simple assessment of the global long term supply of the rare earth elements by using a system dynamics model, Environ. Nat. Resour. Res. 3 (2013) 77–91.
[3] https://www.bgs.ac.uk/sosminerals/downloads/scienceAndImplementationPlan.pdf (Accessed 25/10/17)
[4] Z. Baolu, Z. Li, C. Chen, Global potential of rare earth resources and rare earth demand from clean technologies, Minerals 7 (2017) 1–14.
[5] T. Okada, Y. Ehara, M. Ogawa, Adsorption of europium ion on smectites and fluortetrasilicic mica, Clays Clay Miner. 55 (2007) 348–353.

[6] H.M. Gad, N.S. Awwad, Factors affecting on the sorption/desorption of Eu (III) using activated carbon, Sep. Sci. Technol. 42 (2007) 3657–3680.
[7] M. Bouby, J. Lutzenkirchen, K. Dardenne, T. Preocanin, M.A. Denecke, R. Klenze, H. Geckeis, Sorption of Eu(III) onto titanium dioxide: Measurements and modeling, J. Colloid Interface Sci. 350 (2010) 551–561.
[8] D. Li, Y. Bai, X. Sun, S. Liu, Advances in solvent extraction and separation of rare earths, in: I.M. London, J.R. Goode, G. Moldoveanu, M.S. Rayat (Eds.), 52nd Conference of Metallurgists (COM), Canadian Institute of Mining Metallurgy and Petroleum, Montreal, Canada, 2013, pp. 367–374.
[9] J.E. Quinn, K.H. Soldenhoff, G.W. Stevens, Solvent extraction of rare earth elements using a bifunctional ionic liquid. Part 2: Separation of rare earth elements, Hydrometallurgy. 169 (2017) 621–628.
[10] C. Yan, C. Liao, J. Jia, M. Wang, B. Li, Comparison of economical and technical indices on rare earth separation processes of bastnasite by solvent extraction, J. Rare Earths 17 (1999) 58–63.
[11] F. Xie, T.A. Zhang, D. Dreisinger, F. Doyle, A critical review on solvent extraction of rare earths from aqueous solutions, Miner. Eng. 56 (2014) 10–28.
[12] C. Liao, S. Wu, F. Cheng, S. Wang, Y. Liu, B. Zhang, C. Yan, Clean separation technologies of rare earth resources in China, J. Rare Earths. 31 (2013) 331–336.
[13] R.A. Crane, T.B. Scott, Nanoscale zero-valent iron: future prospects for an emerging water treatment technology, J. Haz. Mater. 211 (2012) 112–125.
[14] C. Noubactep, S. Caré, R.A. Crane, Nanoscale metallic iron for environmental remediation: prospects and limitations, Water Air Soil Pollut. 223 (2012) 1363–1382.
[15] R.M. Ashour, E.-S. Ramy, A.F. Abdel-Magied, A.A. Abdel-Khalek, M.M. Ali, K. Forsberg, A. Uheida, M. Muhammed, J. Dutta, Selective separation of rare earth ions from aqueous solution using functionalized magnetite nanoparticles: kinetic and thermodynamic studies, Chem. Eng. J. 327 (2017) 286–296.
[16] T.B. Scott, M. Dickinson, R.A. Crane, O. Riba, G. Hughes, G. Allen, The effects of vacuum annealing on the structure and surface chemistry of iron nanoparticles, J. Nano Res. 12 (2010) 2081–2092.
[17] R.A. Crane, M. Dickinson, I.C. Popescu, T.B. Scott, Magnetite and zero-valent iron nanoparticles for the remediation of uranium contaminated environmental water, Water Res. 45 (2011) 2931–2942.
[18] R.A. Crane, T.B. Scott, The removal of uranium onto nanoscale zero-valent iron in anoxic batch systems, J. Nanomater. 2014 (2014) 1–12.
[19] R.A. Crane, H. Pullin, J. Macfarlane, M. Silion, I.C. Popescu, M. Andersen, V. Calen, T.B. Scott, Field application of iron and iron-nickel nanoparticles for the ex situ remediation of a uranium bearing mine water effluent, J. Environ. Eng. 141 (2015) 241–259.
[20] S.U. Yesillera, A.E. Eroğlua, T. Shahwanb, Removal of aqueous rare earth elements (REEs) using nano-iron based materials, J. Ind. Eng. Chem. 19 (2013) 898–907.
[21] G.N. Glavee, K.J. Klabunde, C.M. Sorensen, G.C. Hadjipanayis, Chemistry of borohydride reduction of iron(II) and iron(III) ions in aqueous and nonaqueous media, formation of nanoscale Fe, FeB and Fe2B powders, Inorg. Chem. 34 (1995) 28–35.
[22] C.-B. Wang, W.-X. Zhang, Synthesizing nanoscale iron particles for rapid and complete dechlorination of TCE and PCBs, Environ. Sci. Technol. 31 (1997) 2154–2156.
[23] M. Baalousha, Aggregation and disaggregation of iron oxide nanoparticles: influence of particle concentration, pH and natural organic matter, Sci. Tot. Environ. 407 (2009) 2093–2101.
[24] R.A. Crane, H. Pullin, T.B. Scott, The influence of calcium, sodium and bicarbonate on the uptake of uranium onto nanoscale zero-valent iron particles, Chem. Eng. J. 277 (2015) 252–259.
[25] R.A. Crane, T.B. Scott, The effect of vacuum annealing of magnetite and zero-valent Iron nanoparticles on the removal of aqueous uranium, J. Nanotechnol. 2013 (2013) 1–11.
[26] H. Pullin, R.A. Crane, D.J. Morgan, T.B. Scott, The effect of common groundwater anions on the aqueous corrosion of zero-valent iron nanoparticles and associated removal of aqueous copper and zinc, J. Environ. Chem. Eng. 5 (2017) 1166–1173.
[27] R.A. Crane, T.B. Scott, The removal of uranium onto carbon-supported nanoscale zero-valent iron particles, J. Nano. Res. 16 (2014) 1–13.
[28] C. Zhu, G. Fang, D.D. Dionysiou, C. Liu, J. Gao, W. Qin, D. Zhou, Efficient transformation of DDTs with persulfate activation by zero-valent iron nanoparticles: a mechanistic study, J. Hazard. Mater. 5 (2016) 232–241.
[29] R.A. Crane, D.J. Sapsford, Selective formation of copper nanoparticles from acid mine drainage using nanoscale zerovalent iron particles, J. Hazard. Mater. 347 (2018) 252–265.
[30] K. Vijayaraghavan, M. Sathishkumar, R. Balasubramanian, Biosorption of lanthanum, cerium, europium, and ytterbium by a brown marine alga, Turbinaria conoides, Ind. Eng. Chem. Res. 49 (2010) 4405–4411.
[31] S. Liu, L. Zhang, X. Jiang, J. Wang, Y. Chen, Rare Earth Elements Ytterbium (III) Adsorption from Aqueous Solution onto the Nanometer Silica Powders, J. Nanosci. Nanotechnol. 17 (2017) 9101–9107.
[32] C. Xiong, G. Wang, C. Yao, Adsorption of ytterbium (III) from aqueous solution by SQD–85 resin, Trans. Nonferrous Met. Soc. China 21 (2010) 2764–2771.
[33] N. Takeno, Atlas of Eh-pH diagrams, Geol. Surv. Jpn. Open File Rep. 419 (2005) 102.
[34] S.A. Wood, The aqueous geochemistry of the rare-earth elements and yttrium: 1. Review of available low-temperature data for inorganic complexes and the inorganic REE speciation of natural waters, Chem. Geol. 82 (1990) 159–186.
[35] F. Zhao, D. Ren, Z. Cong, H. Sun, The geochemistry of rare earth elements (REE) in acid mine drainage from the Sitai coal mine, Shanxi Province, North China, Int. J. Coal Geol. 70 (2007) 184–192.
[36] L. Lan, W.-X. Zhang, Reactions of nanoscale zero-valent iron with Ni(II): three dimensional tomography of the “hollow out” effect in a single nanoparticle, Environ. Sci. Technol. Lett. 1 (2014) 209–213.
[37] https://xpssimplified.com/elements/lanthanum.php (Accessed 20/10/17)
[38] K. Binnemans, P.T. Jones, B. Blanpain, T. Van Gerven, Y. Pontikes, Towards zero-waste valorisation of rare-earth-containing industrial process residues: a critical review, J. Cleaner Prod. 99 (2015) 17–38.
[39] https://www.ars.usda.gov/oc/images/photos/jun05/d115-1/ (Accessed 08/01/2018)